7-8-2022

Explosive spontaneous emulsification

Xuefei Wu

Gautam Bordia

Robert Streubel

Jaffar Hasnain

Ahmad K. Omar

See next page for additional authors

Authors

Xuefei Wu, Gautam Bordia, Robert Streubel, Jaffar Hasnain, Ahmad K. Omar, Phillip L. Geissler, Dong Wang, Han Xue, Jianjun Wang, and Thomas P. Russell

Explosive spontaneous emulsification

Xuefei Wu[1,2], Gautam Bordia [2,3], Robert Streubel[4,5], Jaffar Hasnain[2,6], Ahmad K. Omar[2,3*], Phillip L. Geissler[6*], Dong Wang[1*], Han Xue[7], Jianjun Wang[7], Thomas P. Russell[1,2,8,9*]

[1]Beijing Advanced Innovation Center for Soft Matter Science and Engineering & State Key Laboratory of Organic-Inorganic Composites, Beijing University of Chemical Technology, Beijing 100029, China

[2]Materials Sciences Division, Lawrence Berkeley National Laboratory, Berkeley, CA 94720, USA

[3]Department of Materials Science and Engineering, University of California, Berkeley, Berkeley, CA 94720, USA

[4]Department of Physics and Astronomy, University of Nebraska-Lincoln, Lincoln, NE 68588, USA

[5]Nebraska Center for Materials and Nanoscience, University of Nebraska-Lincoln, Lincoln, NE 68588, USA

[6]Department of Chemistry, University of California, Berkeley, Berkeley, CA 94720, USA

[7]Beijing National Laboratory for Molecular Science, Institute of Chemistry, Chinese Academy of Sciences, Beijing 100190, China

[8]Polymer Science and Engineering Department, University of Massachusetts, Amherst, MA 01003, USA

[9]Advanced Institute for Materials Research (AIMR), Tohoku University, 2-1-1 Katahira, Aoba, Sendai 980-8577, Japan

*Corresponding author. Email: aomar@berkeley.edu; geissler@berkeley.edu; dwang@mail.buct.edu.cn; russell@mail.pse.umass.edu

Abstract

Spontaneous emulsification, resulting from the assembly and accumulation of surfactants at liquid-liquid interfaces, is an interfacial instability where microdroplets are generated and diffusively spread from the interface until complete emulsification. Here, we show that an external magnetic field can modulate the assembly of paramagnetic nanoparticle surfactants (NPSs) at liquid-liquid interfaces and trigger an oversaturation in the areal density of the NPSs at the interface, as evidenced by the reduction in the interfacial

tension, γ, and corroborated with a magnetostatic continuum theory. Despite the significant reduction in γ, the presence of the magnetic field does not cause stable interfaces to become unstable. Upon rapid removal of the field, however, the stored free energy is released through an explosive ejection of a plume of microdroplets, a dynamical interfacial instability which we term *explosive* spontaneous emulsification. This explosive event rapidly reduces the areal density of the NPSs to its pre-field level, stabilizing the interface. The ability to externally trigger or suppress spontaneous emulsification, through this efficient untapped energy storage and release process, has potential applications for micro-propulsion systems and remotely controlled soft microrobots.

Main Text

Interfacial phenomena are ubiquitous in nature and play a critical role in a plethora of materials engineering[1-3], chemical reaction[4-7], and mass transport processes[8-10]. In all these applications, the interfacial tension, γ, plays a central role in determining the mechanical stability of the liquid-liquid interface. Moreover, changes or gradients in γ can generate a variety of nonequilibrium phenomena including Marangoni flows[11-14] and motion driven by capillary forces. One of the more familiar examples of a nonequilibrium interfacial phenomenon is spontaneous emulsification, i.e., the process by which an unstable liquid-liquid interface spontaneously generates additional surface area by the formation of droplets at the interface and, eventually, an emulsion[15-20].

The use of paramagnetic nanoparticle surfactants (NPSs) provides additional control of surfactant adsorption through the application of an external magnetic field[21-25] (in addition to the more canonical control variables of surfactant concentration and solution chemistry e.g., pH[25-27]). Absent an applied field, adding such NPSs to a system with interfaces results in traditional spontaneous emulsification, the generation of additional interfacial area, due to their

strong surface activity[15]. We report that the application of a constant external magnetic field results in an additional adsorption of NPSs to the interface. However, for conditions where the interface is stable without the field, no instability is observed upon application of the field, despite what appears to be an oversaturated interface. Subsequently, rapidly removing the external field is found to result in an explosive event in which *ferromagnetic* microdroplets are ballistically ejected from the interface. Following this initial explosive emulsification, ferromagnetic microdroplets continue to be released from the parent droplet until the equilibrium NPS surface coverage is restored. This unique interfacial response may provide new insights for the design of micro-propulsion systems[28] and remotely controlled soft microrobots[29,30]. More fundamentally, the use of a magnetic field allows a precise temporal control of nanoparticle assembly at the interface, enabling a systematic interrogation of interfacial stability and phenomena.

Versatile Interfacial Assembly Behavior

Carboxylated 30-nm-diameter paramagnetic nanoparticles (Fe_3O_4-CO_2H) dispersed in an aqueous medium do not assemble at an interface with an apolar solvent, like toluene[31,32]. Dissolving triamine-modified polystyrene (PS-triNH$_2$), a cationic surfactant, in toluene (see

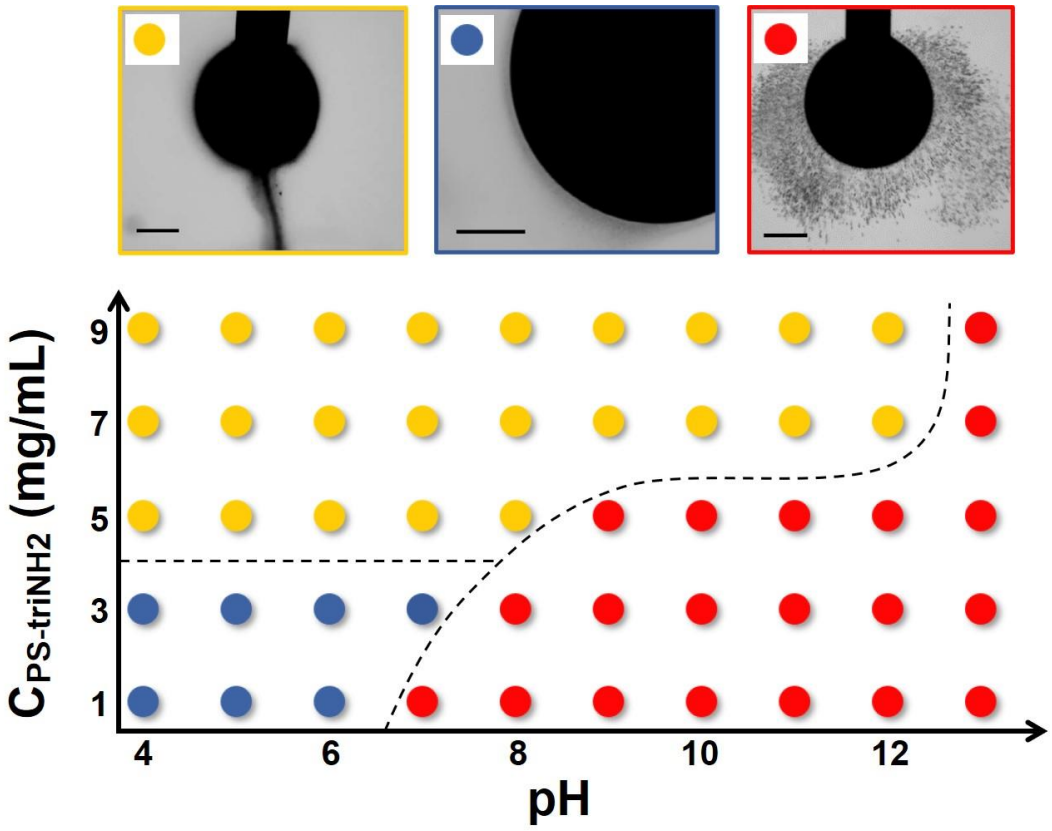

Fig. 1: Interfacial stability diagram. Surfactant concentration ($C_{PS\text{-}triNH2}$) and pH dependencies of spontaneous and explosive emulsification in the strong magnetic field limit (175 kA/m). Spontaneous emulsification (gold circle and dark blue circle) is identified through the constant ejection of microdroplets at lower pH and high surfactant concentration. Explosive emulsification (red circle) occurs only upon rapid removal of the field (the field retraction rates up to tens of mm/s). The dashed line serves as a guide-to-the-eye. Scale bar for the image insets is 500 μm.

Methods), the PS-triNH$_2$ rapidly forms a monolayer at the water/toluene interface and electrostatically interacts with the Fe_3O_4-CO_2H forming paramagnetic NPSs by anchoring a well-defined number of PS-triNH$_2$ to the Fe_3O_4-CO_2H, markedly increasing the binding energy of the nanoparticles to the interface[26,27,33-39]. The NPS surface coverage depends on pH, surfactant and nanoparticle concentrations, and interparticle interactions. At low pH and high surfactant concentration, most amine groups are protonated and strongly anchor the surfactants to the Fe_3O_4-CO_2H. These conditions result in high NPS surface coverage, as indicated by a

significantly reduced γ (Supplementary Fig. 2) and can ultimately result in spontaneous emulsification where a steady stream of microdroplets flows from the base of the parent droplet (Fig. 1, gold circle; Supplementary Video 1) [15]. Spontaneous emulsification can also produce a diffusive ring of microscopic emulsion droplets several tens of micrometers away from the parent drop surface (Supplementary Fig. 3) at lower ligand concentration and pH (Fig. 1, dark blue circle). At higher pH, the binding energy of the NPSs to the interface decreases[26,27], and spontaneous emulsification requires higher surfactant concentrations. For the conditions examined in this work, there exists a wide range of pH and concentrations in which the interface remains stable (see Fig. 1, red circle) in the absence of any applied field. These stable interfaces are the result of a reduced NPS surface coverage in comparison to interfaces that undergo spontaneous emulsification.

Magnetic Field-Induced Interfacial Instability

The paramagnetic nature of the NPSs provides an additional dimension to alter the interfacial

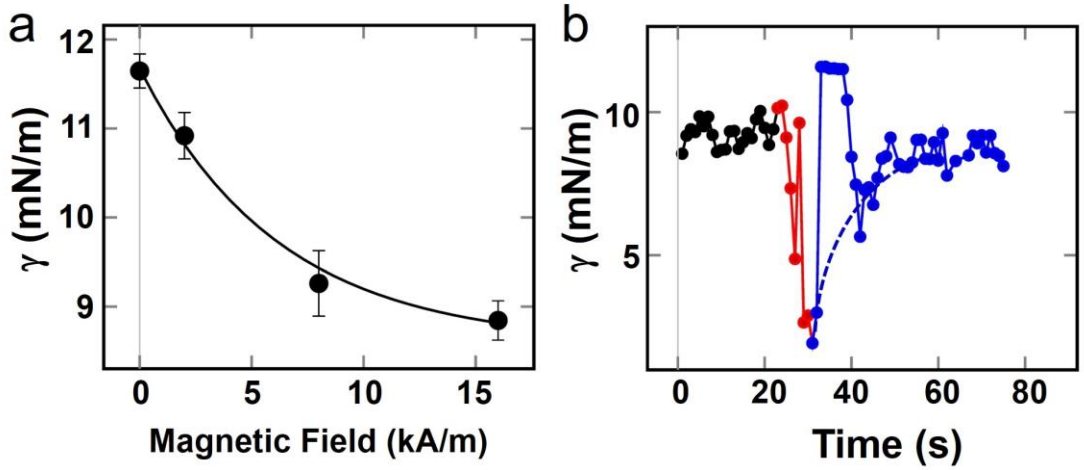

Fig. 2: Magnetic field dependence of interfacial tension, γ. a, Relationship between the equilibrium γ value and the applied magnetic field. **b**, Temporal evolution of γ between the aqueous and toluene phase before (black line), during (red line), and after (blue solid/dashed line) the magnetization of nanoparticle surfactants by an external, non-uniform magnetic field (~175 kA/m) that can deform the aqueous droplet and lead to a rapid increase in γ after the field removed. The concentrations of Fe_3O_4-CO_2H and PS-triNH_2 are 1 mg/mL; pH of aqueous phase is 7.

surface coverage. Application of a strong dc magnetic field (175 kA/m) is hypothesized to alter the driving force for paramagnetic NPS interfacial assembly. For systems undergoing

spontaneous emulsification prior to application of the field (i.e., low pH and high surfactant concentration), emulsification continues and appears slightly suppressed by the presence of the field (Supplementary Fig. 9).

The influence of an external field is noticeably different for systems that are stable in the absence of the field. Figure 2(a) reveals γ to be a monotonically decreasing function of applied field strength. This trend suggests that the magnetic field increases the population of NPS at the interface.

Explosive Emulsification Mechanics

We leverage computer simulations and continuum theory to reveal the precise nature of this field-induced driving force for the migration of NPSs to the interface. A representative equilibrium configuration of dipolar magnetic particles confined to the surface of a sphere (representing the parent droplet) in the presence of a uniform magnetic field is obtained from computer simulations (see SI) and depicted in Fig. 3a. The polarization magnitude of nanoparticles is spatially inhomogeneous along the droplet's surface, with a greater degree of

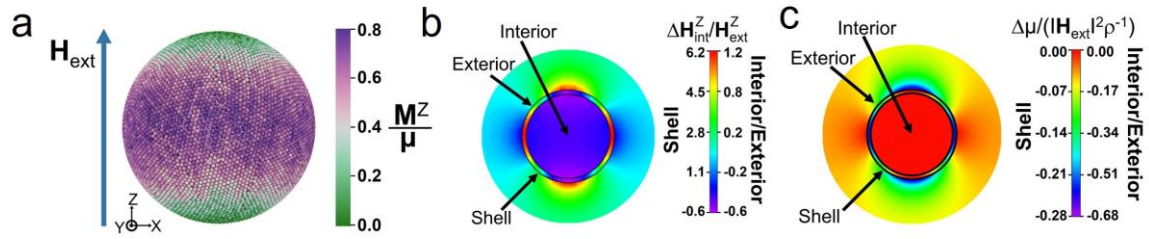

Fig. 3: Thermodynamics of interfacial magnetic dipolar particles. a, Instantaneous simulation configuration of dipolar magnetic particles bound to a spherical surface (50 times larger in diameter than the particles with a surface areal fraction of $\eta = 0.8$) in the presence of a uniform magnetic field. The magnetic field strength is kept weak to facilitate a comparison with linear response theory. **b**, Spatial distribution of the interfacial particle induced field computed in simulations (see SI for details) reveals a spatially inhomogeneous magnetic environment, in agreement with linear response theory (SI). **c**, Linear response prediction for the spatial distribution of the magnetic contribution to the nanoparticle chemical potential. Here we take a magnetic permeability $\varepsilon = 50$ and shell thickness to droplet diameter ratio to be 1:50. Results for thinner shells and other permeabilities give qualitatively similar results.

polarization along the field direction near the droplet equator. The magnetic field generated by

the interfacial dipolar particles is shown in Fig. 3b and reveals significant and nearly uniform magnetic screening of the droplet interior. This screening effect, together with the enhanced polarizability of a particle within the dense shell, results in a significant driving force for particle migration to the interface. Linear response theory confirms these findings (see SI) and allows us to provide a more direct measure of the driving force for interfacial particle migration through the magnetic chemical potential (Fig. 3c).

Despite the enhanced NPS surface coverage resulting in what can be up to an order of magnitude decrease in the γ from the pre-field value, the aqueous droplets remain stable while the field remains present. For systems that were stable but near the emulsification boundary in the absence of the field, one might expect that the field-induced increase in interfacial NPS coverage would provide the requisite driving force for emulsification. Nevertheless, emulsification was not observed despite the observed reduction of γ and the proximity to the emulsification boundary.

The apparent stability of these interfaces has several possible origins. One is that the interface, despite its high NPS coverage, is fully equilibrated and thus truly stable. The stability criteria for an interface are sensitive to the in-plane interactions between interfacial NPSs (or more directly the in-plane pressure exerted by the NPSs)[15]. The magnetic field acts to polarize the magnetic dipoles in the field-direction, which in turn alters the nanoparticle microstructure. While this undoubtedly affects the in-plane pressure tensor, the degree to which this occurs is presently unclear. An alternative and intriguing possibility is that the droplet is metastable due to the NPS microstructure introducing a barrier to emulsification, the globally stable system configuration. As a well-established example of such metastability, liquid-liquid interfaces that are maximally packed or "jammed" with NPSs can persist indefinitely and exhibit solid-like properties[25-27,35]. A hallmark of these structured liquids is the development of an elastic response to interfacial deformation. In the present case of magnetic NPSs, however, the surface

coverage is below the threshold for jamming as determined from wrinkling experiments.

Magnet Retraction Rate Dependence

At chemical conditions where the interface is stable in the absence of a field, application and removal of the magnetic field can lead to different scenarios depending on the field retraction rate. Removing the field introduces a thermodynamic driving force for the desorption of the excess NPSs back into the aqueous parent droplet until the equilibrium coverage is restored. As a result, removing the field quasi-statically (i.e., reversibly removing the external field) should result in the steady desorption of NPS into the aqueous phase and a return to stable interface.

If the field is instead removed at a finite rate, nonequilibrium dynamical effects may dominate the response. Since the degree of paramagnetic NPS adsorption increases with the magnetic field strength (Supplementary Fig. 4e), we focus on strong magnetic field strengths (~175 kA/m) with a magnetization time of ~10 s before retracting the field (see Methods). Rapidly removing the external magnetic field allows for probing the irreversible limit and observing a forceful ejection of microdroplets after a short delay, i.e., within two seconds after removal of the field (Fig. 1, Supplementary Fig. 4, Supplementary Video 2).

At the fastest removal rate, tens of thousands of microdroplets (Fig. 4a), ~4 μm in diameter, are ejected at a velocity of ~3.7 mm/s (Fig. 4c) and continue their persistent motion over 1-2 mm away from the parent droplet surface. This explosive event stabilizes the interface, reflected in the restoration of γ to its pre-field values 10 seconds after removing the field (Fig. 2b). Decreasing the field removal rate monotonically reduces the number of ejected microdroplets and their ejection velocity (Fig. 4c) and increases the delay time (Fig. 4b) between field removal and the explosive event. The diminishment of this explosive event with decreasing field removal rate is consistent with our expectation of no explosive behavior in the

quasi-static limit.

While the ejection velocities of these microdroplets can be extraordinarily large, the colloidal

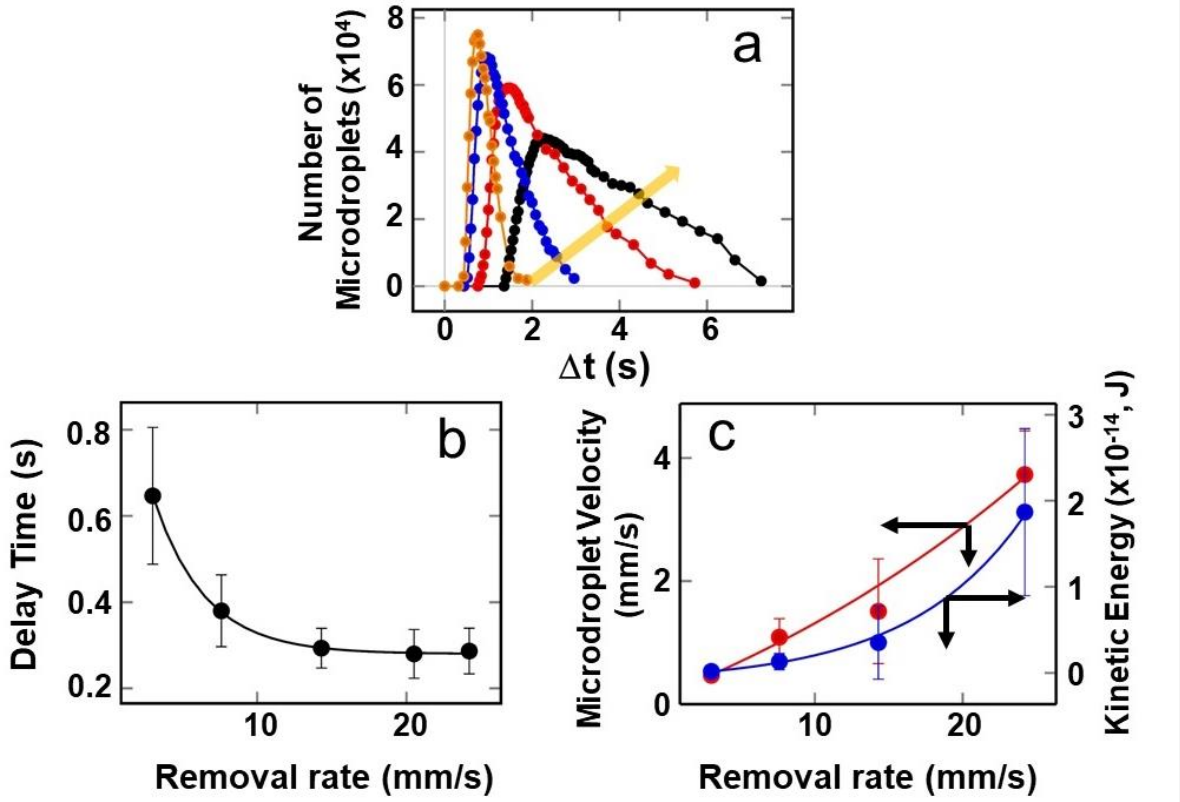

Fig. 4: Influence of magnet retraction rate on explosive emulsification. a, Temporal evolution of the number of explosives produced after withdrawal of the bar magnet at various rates, 3.0 mm/s (black), 7.6 mm/s (red), 14.6 mm/s (blue) and 24.2 (orange). **b,** Delay time for onset of explosive spontaneous emulsification and, **c**, initial velocity and total kinetic energy as a function of retraction velocity of bar magnet. The concentrations of Fe_3O_4-CO_2H and PS-triNH_2 are 1 mg/mL; pH of aqueous phase is 7.

scale of these droplets and the viscosity of the oil would suggest that low-Reynolds number physics are at play and inertial effects are negligible. The persistent motion for these large length scales is therefore likely the result of a persistent force acting on the microdroplets. Magnetic dipolar forces between the parent and microdroplets could provide an initial ejective force, but the ejected microdroplets would rapidly reorient to alleviate such a repulsion. The long-range nature of the force apparently propelling microdroplets is highly suggestive of an electrostatic origin, which may be the result of overcharging the interface upon field removal. The ballistic ejection of microdroplets may also be due to oil radially flowing outward from

the interface because of the latent heat released from the interface upon rapidly removing the field. In this scenario, the drag force from the flowing oil acts to persistently propel the microdroplets away from the interface. Elucidating the precise mechanism for the dynamical explosion is the subject of ongoing work.

Characterization of Microdroplets

The microdroplets produced during explosive spontaneous emulsification and also spontaneous emulsification have a remnant magnetization ,e.g., the remnant magnetization of microdroplets with an average diameter of ~4 μm is found to be ~1.7×10^{-16} A.m^2, calculated using the methods mentioned in ref. 36, and a sizable coercive field (ferromagnetism)[36,40-42] as verified by their rotation in the presence of an external rotating magnetic field (Supplementary Video 3 , Fig. 5b). Previously, the development of ferromagnetism was associated with the jamming of paramagnetic NPSs at the interface.[25,36] This raises the intriguing possibility that despite the parent droplets being decidedly below the jamming transition, the microdroplets generated during explosive emulsification may have a NPS surface coverage that exceeds that of the parent droplet. In the long-time limit and in the absence of a field, these droplets should eventually merge with the parent droplet. The stability as evidenced by the long lifetime of the microdroplets, along with their ferromagnetism, supports the conclusion that they are in fact jammed (Fig. 5b, 5c).

As noted above, high surfactant concentrations significantly reduce γ and promote, in the absence of a magnetic field, spontaneous emulsification. This is evidenced by the microdroplets streaming off the base of the drop under the influence of gravity. The shape of the stream is highly dependent on pH (Fig. 5a). At low pH, the stream bows upward as the microdroplets leave the drop, and, falls straight downwards at high pH. This difference arises from the difference in the size of the microdroplets (as determined by light scattering) (Fig. 5c). Although the density of microdroplets is close to the density of water (1 g/cm^3) and, therefore,

greater than that of the surrounding medium (0.867 g/cm^3), the shape of the stream is still affected by the number and size of the microdroplets produced, due, more than likely, to friction.

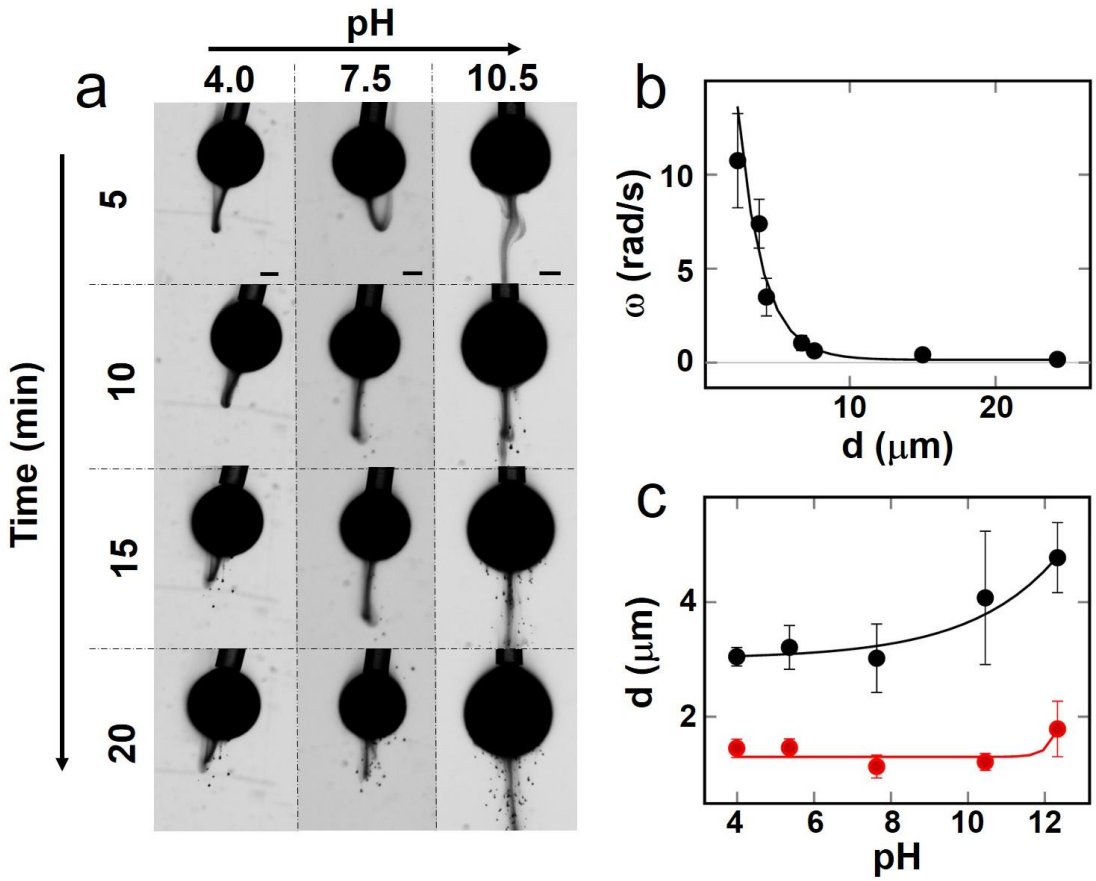

Fig. 5: Spontaneous emulsification of aqueous droplets at high surfactant concentration. **a**, Snapshots of an aqueous droplet with different pH in the oil phase. Scale bar is 500 μm. **b**, Effect of microdroplet size d on the angular frequency ω. The driving angular frequency is 80 rpm. **c**, Average diameter of the microdroplets as a function of pH. The black and red curves refer to fresh and 35-day old, respectively. The concentrations of Fe_3O_4-CO_2H and PS-triNH_2 are 1 mg/mL and 7 mg/mL, respectively. The pH of the aqueous phase is 7.

An optical image of the microdroplets suspended in the oil phase is shown in Supplementary Fig. 7. Except for large droplets that sediment due to gravity (Supplementary Fig. 8), the microdroplets are stable for at least one month without coalescence or loss of their magnetization. After this time, the microdroplets shrink to half their original size (Fig. 5c).

Conclusions

In conclusion, assemblies of paramagnetic NPSs at the oil/water interface were brought into an

oversaturated using an external dc magnetic field. Upon rapid removal of the field, the stored free energy is released through *explosive* spontaneous emulsification, a dynamical interfacial instability where an explosive ejection of a plume of ferromagnetic microdroplets from the interface occurs**.** The potential energy of the parent drop and ejection velocities of the microdroplets were tunable by changing the pH, surfactant concentration, and rate of removal of the permanent magnet from the drop. These findings open new opportunities in designing autonomous propelled systems and has the potential to impact micro-propulsion in medical, soft robotic and other micro-actuated systems.

Methods

Preparation of paramagnetic nanoparticle surfactants at the interface. The negatively charged carboxylic acid-functionalized iron oxide nanoparticles (Fe_3O_4-CO_2H) (Ocean NanoTech) with the diameter of ~30 nm were dispersed in deionized water to form the aqueous dispersion that was injected into the oil phase by the syringe to form a pendant liquid droplet. One monolayer of oleic acid and one monolayer of amphiphilic polymer, totaling ~4 nm, surrounded the ~22 nm-sized magnetic core. The ω-(diethylene triamine)-terminated polystyrene (PS-triNH_2, Mw = 1200 g/mol) (Polymer Source) was dissolved in toluene to interact with Fe_3O_4-CO_2H nanoparticles, forming the magnetic NPSs at the interface. The Fe_3O_4-CO_2H concentration remained 1 mg/mL; the concentration of PS-triNH_2 ranged from 1 to 9 mg/mL. All nanoparticle dispersions were used without further purification and diluted to the required concentration using deionized water. The pH of the aqueous dispersions was adjusted using 1.0 M NaOH or HCl.

Interfacial tension measurement. A tensiometer (Krüss DSA30) was used to measure γ

between water and toluene via the pendant drop method. The time dependence of γ was recorded after the aqueous droplet had been injected into the oil phase. The volume of the aqueous droplet was ~5 μL, and the measurement time was up to 3000 s. A homemade Helmholtz coil was used to magnetize the magnetic NPSs in a uniform magnetic field up to 16 kA/m. The droplet volume remained constant in the presence of the magnetic field, indicating that the heat generated by the coil and its effect on the assembly were negligible. The distortion of the shape was studied with a magnetic field gradient to attract the droplet.

Optical observation of the interfacial behavior. A digital camera on a tensiometer was used to visualize the macroscopic behavior of the magnetic NPSs at and near the interface, with the pH of aqueous phase and surfactant concentration varied. A strong bar magnet (NdFeB) was used to magnetize the droplet; the magnetic field strength and direction were the same for all measurements. The droplets were exposed for 10 s to a magnetic field of ~175 kA/m.

Microscopic characterization of the microdroplets. The micromorphology of the microdroplets was characterized by polarized optical microscopy (ZEISS Imager.A2). The diameter of the microdroplet suspended in toluene was detected by means of dynamic light scattering (Malvern Zetasizer Nano Series ZS90), and the microdroplet dispersions were prepared by spontaneously forming microdroplets at the interface of the hanging aqueous droplet in the surrounding oil phase for 3 h. The volumes of the droplet and oil phase were ~5 μL and ~2 mL, respectively. The upper layer of the microdroplet dispersion was used to measure the microdroplet size without additional procedures.

Controllable retraction rate of the magnet. A homebuilt stepping motor was used to control the speed of retraction of a NdFeB magnet that was attached to a translation stage. The motor speed was varied up to 1000 rpm equivalent to a velocity of 3 to 24.2 mm/s. The magnet was

mechanically fixed to the stage to ensure the same magnetic field strength and direction for all measurements.

Data Availability

All data supporting the findings of this study are available within the Article and the Supplementary Information, and from the corresponding author on reasonable request.

References

1 Horiuchi, S., Matchariyakul, N., Yase, K. & Kitano, T. Morphology development through an interfacial reaction in ternary immiscible polymer blends. *Macromolecules* **30**, 3664-3670 (1997).

2 Zhu, Y. P., Guo, C., Zheng, Y. & Qiao, S. Z. Surface and interface engineering of noble-metal-free electrocatalysts for efficient energy conversion processes. *Acc. Chem. Res.* **50**, 915-923 (2017).

3 Zhang, S. *et al.* Carbon nanotube/carbon composite fiber with improved strength and electrical conductivity via interface engineering. *Carbon* **144**, 628-638 (2019).

4 Astumian, R. D. & Chock, P. B. Interfacial reaction dynamics. *J. Phys. Chem.* **89**, 3477-3482 (1985).

5 Sawarkar, C. S. & Juvekar, V. A. Kinetics of an interfacial reaction. Hydroxide ion catalyzed C-alkylation of phenylacetonitrile. *Ind. Eng. Chem. Res.* **35**, 2581-2589 (1996).

6 Ge, J., Chu, J., Jiang, J., Yan, Y. & Yang, P. The interfacial reaction at ITO back contact in kesterite CZTSSe bifacial solar cells. *ACS Sustainable Chem. Eng.* **3**, 3043-3052 (2015).

7 Xie, C., Niu, Z., Kim, D., Li, M. & Yang, P. Surface and interface control in nanoparticle catalysis. *Chem. Rev.* **120**, 1184-1249 (2020).

8 hunsel, J. V. & Joos, P. Steady-state dynamic interfacial tensions of 1-alkanols during mass transfer across the hexane/water interface. *Langmuir* **3**, 1069-1074 (1987).

9 Goodenough, J. B. & Park, K. S. The Li-ion rechargeable battery: a perspective. *J. Am. Chem. Soc.* **135**, 1167-1176 (2013).

10 Nagl, R., Zimmermann, P. & Zeiner, T. Interfacial mass transfer in water–toluene systems. *J. Chem. Eng. Data* **65**, 328-336 (2019).

11 Tian, D. *et al.* Fast responsive and controllable liquid transport on a magnetic fluid/nanoarray composite interface. *ACS Nano* **10**, 6220-6226 (2016).

12 Hwang, H., Papadopoulos, P., Fujii, S. & Wooh, S. Driving droplets on liquid repellent surfaces via light‐driven marangoni propulsion. *Adv. Funct. Mater.* **32**, 2111311 (2022).

13 Gugliotti, M., Baptista, M. S., Politi, M. J., Silverstein, T. P. & Slater, C. D. Surface tension gradients induced by temperature: the thermal marangoni effect. *J. Chem. Educ.* **81**, 824-826 (2004).

14 Hooshanginejad, A. & Jung, S. Buoyancy-Marangoni Fingering of a Miscible Spreading Drop. *Symmetry* **14**, 425 (2022).

15 Hasnain, J. *et al.* Spontaneous emulsification induced by nanoparticle surfactants. *J. Chem. Phys.* **153**, 224705 (2020).

16 Granek, R., Ball, R. C. & Cates, M. E. Dynamics of spontaneous emulsification. *J. Phys.*

II **3**, 829-849 (1993).
17 Zhu, J. & Hayward, R. C. Hierarchically structured microparticles formed by interfacial instabilities of emulsion droplets containing amphiphilic block copolymers. *Angew. Chem.* **120**, 2143-2146 (2008).
18 Guttman, S. *et al.* How faceted liquid droplets grow tails. *Proc. Natl Acad. Sci. USA* **113**, 493-496 (2016).
19 Zhu, J. & Hayward, R. C. Spontaneous generation of amphiphilic block copolymer micelles with multiple morphologies through Interfacial Instabilities. *J. Am. Chem. Soc.* **130**, 7496-7502 (2008).
20 Ku, K. H. *et al.* Particles with Tunable Porosity and Morphology by Controlling Interfacial Instability in Block Copolymer Emulsions. *ACS nano* **10**, 5243-5251 (2016).
21 Zhang, Z. *et al.* Guiding kinetic trajectories between jammed and unjammed states in 2D colloidal nanocrystal-polymer assemblies with zwitterionic ligands. *Sci. Adv.* **4**, eaap8045 (2018).
22 Saini, A. *et al.* Magnetic Particle Self-Assembly at Functionalized Interfaces. *Langmuir : the ACS journal of surfaces and colloids* **37**, 4064-4071 (2021).
23 Singh, G. *et al.* Magnetic field-induced self-assembly of iron oxide nanocubes. *Faraday Discuss.* **181**, 403-421 (2015).
24 Martinez-Pedrero, F. Static and dynamic behavior of magnetic particles at fluid interfaces. *Adv. Colloid Interface Sci.* **284**, 102233 (2020).
25 Liu, X. *et al.* Reconfigurable ferromagnetic liquid droplets. *Science* **365**, 264–267 (2019).
26 Cui, M., Emrick, T. & Russell, T. P. Stabilizing liquid drops in nonequilibrium shapes by the interfacial jamming of nanoparticles. *Science* **25**, 460-463 (2013).
27 Liu, X. *et al.* Liquid tubule formation and stabilization using cellulose nanocrystal surfactants. *Angew.Chem.* **129**, 12768-12772 (2017).
28 Micci, M. M. *Micropropulsion for small spacecraft*. (American Institute of Aeronautics and Astronautics, 2000).
29 Xie, H. *et al.* Reconfigurable magnetic microrobot swarm: multimode transformation locomotion and manipulation. *Sci. Robot.* **4**, eaav8006 (2019).
30 Halder, A. & Sun, Y. Biocompatible propulsion for biomedical micro/nano robotics. *Biosens. Bioelectron.* **139**, 111334 (2019).
31 Marinova, K. G. *et al.* Charging of oil-water interfaces due to spontaneous adsorption of hydroxyl ions. *Langmuir* **12**, 2045-2051 (1996).
32 Pullanchery, S., Kulik, S., Rehl, B., Hassanali, A. & Roke, S. Charge transfer across C-H•••O hydrogen bonds stabilizes oil droplets in water. *Science* **374**, 1366-1370 (2021).
33 Wu, X. *et al.* Nanorod–surfactant assemblies and their interfacial behavior at liquid–liquid interfaces. *ACS Macro Lett.* **8**, 512-518 (2019).
34 Huang, C. *et al.* Bicontinuous structured liquids with sub-micrometre domains using nanoparticle surfactants. *Nat. Nanotechnol.* **12**, 1060-1063 (2017).
35 Hou, H. *et al.* Interfacial activity of amine-functionalized polyhedral oligomeric silsesquioxanes (POSS): a simple strategy to structure liquids. *Angew. Chem.* **58**, 10142-10147 (2019).
36 Wu, X. *et al.* Ferromagnetic liquid droplets with adjustable magnetic properties. *Proc. Natl Acad. Sci. USA* **118**, e2017355118 (2021).
37 Shi, S. *et al.* Liquid letters. *Adv. Mater.* **30**, 1705800 (2018).
38 Forth, J. *et al.* Reconfigurable printed liquids. *Adv. Mater.* **30**, e1707603 (2018).
39 Huang, C. *et al.* The interfacial assembly of polyoxometalate nanoparticle surfactants. *Nano Lett.* **18**, 2525-2529 (2018).
40 Streubel, R., Liu, X., Wu, X. & Russell, T. P. Perspective: ferromagnetic liquids.

Materials **13**, 2712 (2020).
41 Theis-Bröhl, K. *et al.* Self-assembled layering of magnetic nanoparticles in a ferrofluid on silicon surfaces. *ACS Appl. Mater. Interfaces* **10**, 5050-5060 (2018).
42 Taheri, S. M. *et al.* Self-assembly of smallest magnetic particles. *Proc. Natl Acad. Sci. USA* **112**, 14484-14489 (2015).

Acknowledgements

The experiments were supported by the U.S. Department of Energy, Office of Science, Office of Basic Energy Sciences, Materials Sciences and Engineering Division under Contract No. DE-AC02-05-CH11231 within the Adaptive Interfacial Assemblies Towards Structuring Liquids program (KCTR16). The authors also acknowledge the support of the Beijing Advanced Innovation Center for Soft Matter Science and Engineering at the Beijing University of Chemical Technology.

Author contribution

X.W. and T.P.R. designed the experiments. X.W. and H.X. performed experiments. G.B., R.S., J.H., A.K.O and P.L.G. developed the theoretical background and performed the simulations. X.W., G.B., R.S., J.H., A.K.O., P.L.G., D.W., H.X., J.W. and T.P.R. had discussions on the results and analysis. X.W., A.K.O, P.L.G. and T. P. R. drafted the manuscript, and all the authors were involved in the discussion of results and the final manuscript editing.

Corresponding authors

Correspondence to Ahmad K. Omar, Phillip L. Geissler, Dong Wang or Thomas P. Russell

Competing interests

The authors declare no competing interests.

Additional information

Publisher's note Springer Nature remains neutral with regard to jurisdictional claims in published maps and institutional affiliations.

Supplementary Materials for

Explosive spontaneous emulsification

Xuefei Wu, Gautam Bordia, Robert Streubel, Jaffar Hasnain, Ahmad K. Omar*, Phillip L. Geissler*, Dong Wang*, Han Xue, Jianjun Wang, Thomas P. Russell*

Correspondence to: aomar@berkeley.edu; geissler@berkeley.edu; dwang@mail.buct.edu.cn; russell@mail.pse.umass.edu

This PDF file includes:

Other Supplementary Materials for this manuscript include the following:

Supplementary Text

To estimate the response of interfacial nanoparticles (NPs) to an external magnetic field, we have: (i) solved magnetostatic continuum equations within a linear response approximation, and; (ii) performed computer simulations of interacting magnetic particles on the surface of a sphere. Results of these two calculations, which agree qualitatively, are shown in Fig. 3 of the main text. Details of these calculations are presented here in addition to further analysis.

Linear Response Theory

An isolated paramagnetic NP (or a freely rotating superparamagnetic NP) will develop a nonzero average magnetic dipole $\langle \mathbf{M} \rangle_{\mathbf{H}_{ext}}$ in the presence of an external magnetic field $\mathbf{H}_{ext}$. The expected linear growth of $|\langle \mathbf{M} \rangle_{\mathbf{H}_{ext}}|$ with $|\mathbf{H}_{ext}|$ can be described by an effective free energy

$$F(\mathbf{M}) = \frac{1}{2\alpha} |\mathbf{M}|^2 - \mathbf{H}_{ext} \cdot \mathbf{M}$$

with polarizability $\alpha = \beta \langle |\mathbf{M}|^2 \rangle_0$, where $\beta = (k_B T)^{-1}$ and T is temperature. The chemical potential associated with this particle's dipole fluctuations is

$$\mu = k_B T \ln \int d\mathbf{M} e^{-\beta F(\mathbf{M})} = \text{const} - \frac{\alpha}{2} |\mathbf{H}_{ext}|^2$$

where the constant is independent of $\mathbf{H}_{ext}$. We will focus exclusively on changes in μ due to the external field, $\Delta\mu = \mu(\mathbf{H}_{ext}) - \mu(0)$. For the isolated NP, we then have

$$\Delta\mu = -\frac{\alpha}{2} |\mathbf{H}_{ext}|^2 \quad \text{(S1)}$$

A dense collection of such particles, within a volume V, can be viewed on sufficiently large length scales as a polarizable continuum with free energy

$$F[\mathbf{m}(\mathbf{r})] = \frac{1}{2} \int d\mathbf{r} \int d\mathbf{r}' \, \mathbf{m}(\mathbf{r}) \cdot \left[\left((\rho\alpha)^{-1} - \frac{4\pi}{3} \right) \mathbf{I} \delta(\mathbf{r} - \mathbf{r}') + \nabla\nabla' \frac{1}{|\mathbf{r} - \mathbf{r}'|} \right] \cdot \mathbf{m}(\mathbf{r}') - \int d\mathbf{r} \mathbf{H}_{ext} \cdot \mathbf{m}(\mathbf{r}) \quad \text{(S2)}$$

where ρ is the number density of NPs and $\mathbf{m}(\mathbf{r})$ is the net dipole per unit volume in a small region at position $\mathbf{r}$. The dipole-dipole interaction tensor $\nabla\nabla' |\mathbf{r} - \mathbf{r}'|^{-1}$ gives a singular but integrable self-interaction at $\mathbf{r} = \mathbf{r}'$, whose contribution is subtracted in the first term of Eq. S2. The average behavior of this linear response model is equivalent[1-3] to solutions of

$$\nabla \cdot \mathbf{H} = 0 \quad \text{(S3)}$$

where

$$\mathbf{H} = \mathbf{H}_{ext} - \int d\mathbf{r}' \nabla\nabla' \frac{1}{|\mathbf{r} - \mathbf{r}'|} \cdot \mathbf{m}(\mathbf{r}') \quad \text{(S4)}$$

is the total magnetic field at $\mathbf{r}$, accompanied by the linear response relation

$$\mathbf{m}(\mathbf{r}) = \frac{\varepsilon - 1}{4\pi} \mathbf{H}(\mathbf{r})$$

The relative magnetic permeability ε is determined by microscopic parameters through the magnetic analog of the Clausius-Mossotti equation, $4\pi\rho\alpha/3 = (\varepsilon - 1)/(\varepsilon + 2)$. (This permeability is conventionally denoted μ, a symbol we reserve for chemical potential. The ε-notation is a reminder that the entire linear response calculation would proceed identically for a collection of electric dipoles, for which ε represents the dielectric constant.)

Boundary conditions must be satisfied at interfaces between V and regions $\tilde{V}$ lacking NPs

$$\varepsilon \mathbf{H}_V \cdot \hat{\mathbf{n}} = \mathbf{H}_{\tilde{V}} \cdot \hat{\mathbf{n}} \quad \text{(S5)}$$

$$\mathbf{H}_V \cdot \hat{\mathbf{t}} = \mathbf{H}_{\tilde{V}} \cdot \hat{\mathbf{t}} \quad \text{(S6)}$$

$\hat{\mathbf{n}}$ and $\hat{\mathbf{t}}$ are unit vectors pointing normal and tangential, respectively, to the local surface.

As an idealization of paramagnetic NPs adsorbed at a droplet interface, we consider a polarizable spherical shell, with inner radius a and outer radius b, centered at the origin (see

Supplementary Fig. 1). We take the external magnetic field, $\mathbf{H}_{ext} = H_{ext}\hat{\mathbf{z}}$ = const, to be uniform and oriented along the polar direction $\hat{\mathbf{z}}$.

For a time-independent external field, $\nabla \times \mathbf{H} = 0$, so that $\mathbf{H}$ can be written as the gradient of a scalar potential,

$$\mathbf{H}(\mathbf{r}) = -\nabla\phi(\mathbf{r})$$

We must therefore solve a Laplace equation,

$$\nabla^2\phi(\mathbf{r}) = 0$$

within each of three regions, namely "in" ($r < a$), "shell" ($a \le r \le b$), and "out" ($r > b$). The boundary conditions (S6) are supplemented by the requirement that $\mathbf{H}(\mathbf{r})$ asymptotically approaches $\mathbf{H}_{ext}$ at large r.

The axial symmetry of this problem permits a general solution to the Laplace equation in terms of r and the polar angle $\theta = \cos^{-1}(\hat{\mathbf{z}}\cdot\hat{\mathbf{r}})$,

$$\phi(r, \cos\theta) = \sum_{l=0}^{\infty}\left[B_l r^l + C_l r^{-(l+1)}\right]P_l(\cos\theta)$$

where $P_l(x)$ are Legendre polynomials. B_l and C_l are constant within each of the three regions but may change discontinuously at the boundaries between them. For $l = 0$ and $l > 1$, boundary conditions are satisfied with $B_l = C_l = 0$ and so we will henceforth omit the subscript l with $l = 1$ implied. The solution to this boundary value problem is then determined by the six remaining coefficients, i.e., values of B and C in the exterior, shell, and interior regions:

$$B^{\text{shell}} = -3|\mathbf{H}_{\text{ext}}|\left[\varepsilon + 2 - 2\left(\frac{a}{b}\right)^3\frac{(\varepsilon-1)^2}{2\varepsilon+1}\right]^{-1} \quad \text{(S7)}$$

$$C^{\text{shell}} = a^3\frac{\varepsilon-1}{2\varepsilon+1}B^{\text{shell}} \quad \text{(S8)}$$

$$B^{\text{in}} = B^{\text{shell}} + C^{\text{shell}}a^{-3} = B^{\text{shell}}\left(1 + \frac{\varepsilon-1}{2\varepsilon+1}\right) \quad \text{(S9)}$$

$$C^{\text{in}} = 0 \quad \text{(S10)}$$

$$C^{\text{out}} = b^3\left[\varepsilon_0 + B^{\text{shell}} + C^{\text{shell}}\,b^{-3}\right] \quad \text{(S11)}$$

$$B^{\text{out}} = -\mathrm{H}_{\text{ext}} \quad \text{(S12)}$$

The resulting total magnetic field follows by differentiation:

$$\mathbf{H} = -\nabla[Br + Cr^{-2}\cos\theta]$$

Giving

$$\mathbf{H}^{\text{in}} = -B^{\text{in}}\hat{\mathbf{z}} \qquad (r < a) \quad \text{(S13)}$$

$$\mathbf{H}^{\text{shell}} = B^{\text{shell}}\hat{\mathbf{z}} - \frac{C^{\text{shell}}}{r^3}\left(\hat{\mathbf{z}} - 3\frac{z}{r}\hat{\mathbf{r}}\right) \qquad (a < \mathrm{r} < b) \quad \text{(S14)}$$

$$\mathbf{H}^{\text{out}} = \mathbf{H}_{\text{ext}}\hat{\mathbf{z}} - \frac{C^{\text{out}}}{r^3}\left(\hat{\mathbf{z}} - 3\frac{z}{r}\hat{\mathbf{r}}\right) \qquad (r > b) \quad \text{(S15)}$$

In the droplet's interior ($r < a$), the external field is uniformly screened by the polarized shell, resulting in a uniform total field (Eq. S13). The field-induced chemical potential shift is therefore also spatially uniform. Adapting Eq. S1, we have

$$\Delta\mu^{in} = -\frac{\alpha}{2}|\mathbf{H}^{\text{in}}|^2 = -\frac{1}{2}\left(\frac{\varepsilon-1}{4\pi\rho}\right)\left(\frac{3}{\varepsilon+2}\right)|\mathbf{H}^{\text{in}}|^2$$

From similar considerations, the dilute region outside the shell has a spatially varying field (Eq. S14) and therefore a spatially varying chemical potential

$$\Delta\mu^{out}(\mathbf{r}) = -\frac{1}{2}\left(\frac{\varepsilon-1}{4\pi\rho}\right)\left(\frac{\mathbf{3}}{\varepsilon+2}\right)|\mathbf{H}^{\text{out}}(\mathbf{r})|^2$$

To compute $\Delta\mu$ for $a < r < b$, we must account for the self-interaction implicit in the continuum expression (Eq. S4). Identifying a subvolume of size ρ^{-1} as the continuum equivalent

of a single particle, we use Eq. S1 with re-normalized α and $\mathbf{H}$ such that $\bar{\alpha} = (\varepsilon - 1)(2\varepsilon + 1)/(12\pi\rho\varepsilon)$ and $\bar{\mathbf{H}}(\mathbf{r}) = 3\varepsilon/(2\varepsilon + 1)\mathbf{H}(\mathbf{r})$[4]

$$\Delta\mu^{shell}(\mathbf{r}) = -\frac{\bar{\alpha}}{2}|\bar{\mathbf{H}}^{\text{shell}}|^2 = -\frac{1}{2}\frac{(\varepsilon-1)(2\varepsilon+1)}{(12\pi\rho\varepsilon)}\left(\frac{3\varepsilon}{2\varepsilon+1}|\mathbf{H}^{\text{shell}}(\mathbf{r})|\right)^2 \quad \text{(S16)}$$

Results of this analysis, shown in Fig. 3C, suggest that paramagnetic NPs experience a chemical potential gradient under an applied magnetic field, driving material away from the screened droplet interior and from the poles of the shell, towards the shell's equator, and towards the polar region of the droplet's exterior. Experimentally, the nanoparticle shell thickness is vanishingly small in comparison to the droplet radius. Upon taking the thin shell limit ($a \to b$) we find the external field is no longer screened by the shell except with-in the shell:

$$\mathbf{H}^{\text{in}} = \mathbf{H}^{\text{out}} = \mathbf{H}_{\text{ext}} \quad \text{(S17)}$$

$$\mathbf{H}^{\text{shell}} = \frac{|\mathbf{H}_{\text{ext}}|}{3\varepsilon}\left[(2\varepsilon+1)\hat{\mathbf{z}} + (\varepsilon-1)\frac{a^3}{r^3}\left(\hat{\mathbf{z}} - 3\frac{z}{r}\hat{\mathbf{r}}\right)\right] \quad \text{(S18)}$$

$$\hat{\mathbf{z}} \cdot \mathbf{H}^{\text{shell}} = |\mathbf{H}_{\text{ext}}|\left[1 - \frac{(\varepsilon-1)}{\varepsilon}\cos^2\theta\right] \quad \text{(S19)}$$

In this limit the chemical potential is spatially uniform except within the shell, where it varies greatly from pole to equator. At the equator μ is much lower than in solution:

$$\Delta\mu^{\text{shell}}_{\text{equator}} = \Delta\mu^{\text{in}}\,\varepsilon\left(\frac{\varepsilon+2}{2\varepsilon+1}\right) < \Delta\mu^{\text{in}} \quad \text{(S20)}$$

By contrast, at the pole μ is higher than in solution:

$$\Delta\mu^{\text{shell}}_{\text{pole}} = \Delta\mu^{\text{in}}\,\frac{1}{\varepsilon}\left(\frac{\varepsilon+2}{2\varepsilon+1}\right) > \Delta\mu^{\text{in}} \quad \text{(S21)}$$

Among the approximations we have made, treating a monolayer of NPs as a continuous field is likely the most aggressive. It is also straightforward to scrutinize with computer simulations of systems comprising discrete NPs, as described in the next section.

Simulations

To verify the predictions from the continuum theory analysis we conduct molecular dynamics simulations of dipolar magnetic nanoparticles constrained to the surface of a sphere. We simulate *N* dipolar particles in a cubic box with volume *V*. Dipolar particles interact with both an effective hard-sphere-like potential and a long-ranged dipolar potential and are also subject to an external magnetic field $\mathbf{H}_{\text{ext}}$.

A liquid droplet is represented as a sphere of radius *R*, centered within the simulation volume, to which particles are bound. More precisely, particles are subject to a potential that is harmonic in radial displacements away from the interface. The potential is sufficiently deep such that all particles irreversibly adsorb onto the interface. The total potential energy of the system *U* is given by the sum of dipolar U_{dp}, volume exclusion U_{ve}, external U_{ext}, and interfacial binding U_{int} potentials with these interactions taking the following functional forms:

$$U = U_{\text{dp}} + U_{\text{ve}} + U_{\text{ext}} + U_{\text{int}} \quad \text{(S22)}$$

$$U_{\text{dp}} = \frac{1}{2}\sum_{i,j\neq i}\frac{1}{r^3}(\mathbf{m}_i \cdot \mathbf{m}_j) - \frac{3}{r^5}(\mathbf{m}_i \cdot \mathbf{r})(\mathbf{m}_j \cdot \mathbf{r}) \quad \text{(S23)}$$

$$U_{\text{ve}} = \frac{1}{2}\sum_{i,j\neq i} 4\varepsilon\left[\left(\frac{\sigma}{r}\right)^{12} - \left(\frac{\sigma}{r}\right)^{6} - \left(\frac{\sigma}{r_c}\right)^{12} + \left(\frac{\sigma}{r_c}\right)^{6}\right] \quad \text{(S24)}$$

$$U_{\text{ext}} = -\sum_i \mathbf{m}_i \cdot \mathbf{H}_{ext} \quad \text{(S25)}$$

$$U_{\text{int}} = \sum_i \kappa(r_i - R_{\text{int}})^2 \quad \text{(S26)}$$

where $\mathbf{r} = \mathbf{r}_\mathbf{i} - \mathbf{r}_\mathbf{j}$ is the displacement vector (with magnitude *r*) between particles *i* and *j* and $\mathbf{m}_i$ is the dipole vector of particle *i* with constant magnitude *m* such that $\mathbf{m}_i = m\boldsymbol{q}_i$ where $\boldsymbol{q}_i$ is a unit vector. Volume exclusion is enforced by a hard-sphere-like interaction, implemented using a

stiff Weeks-Chandler-Anderson (WCA) potential[5], where ε is the Lennard Jones (LJ) interaction energy, σ is the LJ diameter (all references made to the particle diameter refer to the LJ diameter) and $r_c = 2^{1/6}\sigma$ is the cutoff at which the potential is truncated. By setting $\varepsilon = 100k_BT$, we ensure nearly complete volume exclusion with an effective hard-sphere diameter of approximately r_c. Finally, particles are constrained to the interface by choosing a sufficiently large binding energy ($\kappa = 1000k_BT/\sigma^2$) such that the magnitude of the particle's position vector r_i (relative to the origin of the droplet) is equal to the droplet's radius R_{int}. This choice results in all particles in the simulation cell adsorbing to the droplet surface.

Brownian dynamics simulations were used to evolve our system forward in time towards the stationary state. The corresponding translational and rotational equations-of-motion for a particle i are given by

$$\mathrm{m}\ddot{\mathbf{r}}_i = \boldsymbol{\xi}_i^{\,T} - \frac{\partial U}{\partial \mathbf{r}_i} - \gamma^T \dot{\mathbf{r}}_i \tag{S27}$$

$$I\dot{\boldsymbol{\omega}}_i = \boldsymbol{\xi}_i^{\,R} - \frac{\partial U}{\partial \mathbf{q}_i} - \gamma^R \boldsymbol{\omega}_i \tag{S28}$$

where γ^T and γ^R are the translational and rotational drag coefficients, $\dot{\mathbf{r}}_i$ and $\boldsymbol{\omega}_i$ are the translational and angular velocities of particle i, and m and I are the mass and moment of inertia. The stochastic translational and rotational forces ξ^T and ξ^R satisfy the fluctuation dissipation theorem:

$$\langle \boldsymbol{\xi}_i^{\,T}(t) \rangle = \mathbf{0} \tag{S29}$$

$$\langle \boldsymbol{\xi}_i^{\,R}(t) \rangle = \mathbf{0} \tag{S30}$$

$$\langle \boldsymbol{\xi}_i^{\,T}(t)\boldsymbol{\xi}_j^{\,T}(t') \rangle = 2\gamma^T k_B T \delta_{ij} \mathbf{I} \delta(t-t') \tag{S31}$$

$$\langle \boldsymbol{\xi}_i^{\,R}(t)\boldsymbol{\xi}_j^{\,R}(t') \rangle = 2\gamma^R k_B T \delta_{ij} \mathbf{I} \delta(t-t') \tag{S32}$$

where δ_{ij} is the Kronecker delta, $\delta(t-t')$ is the Dirac delta function, and $\mathbf{I}$ is the identity tensor.

The particles' dipole magnitude is scaled to match that of experimental observation for 20 nm super-paramagnetic iron oxide nanoparticles with saturated magnetic dipoles[6]. The dimensionless dipole strength[7] is defined as

$$\Gamma = \frac{m^2}{2\pi\sigma^3 k_B T} \tag{S33}$$

corresponding to the ratio of interaction energy of two perfectly aligned adjacent dipoles to the thermal energy k_BT. For all results shown here we use a dimensionless strength of $\Gamma = 2.84$ as determined from experimental measurements of m. The surface area fraction of particles is held constant at $\eta = Nr_c^2/R^2 = 0.8$. All simulations are conducted with a minimum of 6532 particles in LAMMPS[8].

After an initial equilibration run, a weak uniform external magnetic field is applied uniaxially in the z-direction to align particles. The resulting dipolar orientation is shown in Fig. 3a of the main text. The results indicate a strong spatial dependence of the dipolar orientation, with diminishing alignment with increasing distance from the equator.

To further understand the magnetic environment beyond the droplet surface, we compute the contribution to the magnetic field energy induced by the surface particles in both the interior and exterior of the droplet. We do this by placing ideal dipoles pointing in the field direction throughout the droplet interior, exterior and surface and measuring the net dipolar energy felt by a test particle through interactions with surface particles. The resulting energies are then converted to the z-component of the induced field by dividing by the square of the dipolar magnitude. Due to the spherical symmetry of the system, the induced field can be projected on to the x-z plane as

represented in Fig. 3b (main text). The shell of the droplet displays a quadrupolar interaction field while the magnetic field of the exterior of the droplet exhibits another quadrupolar field that is reversed in polarity relative to the shell's field.

The results from continuum analysis in Fig. 3c (main text) show chemical potential contours similar to the field gradients computed from simulations, shown in Fig. 3b (main text). Importantly, the chemical potential is significantly lower within the shell in comparison to the droplet interior, suggesting a strong magnetic driving force for interfacial assembly in the presence of a uniform magnetic field. This result, in conjunction with the experimentally observed reduction in the interfacial tension with applied field, provides compelling evidence for increased NPS interfacial assembly in the presence of a magnetic field. We note that the chemical potential varies spatially within the shell, with high chemical potential at the poles and a lower chemical potential near the equator. Such a spatially inhomogeneous chemical potential may drive density variations of the NPS at the interface. These induced density variations may be important towards a complete understanding of explosive spontaneous emulsification and is the subject of ongoing investigation.

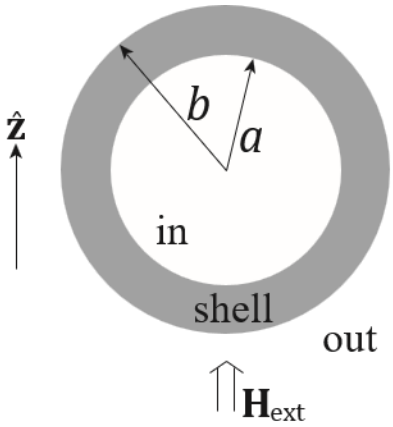

Supplementary Fig. 1. Spherical shell geometry for continuum linear response calculation.

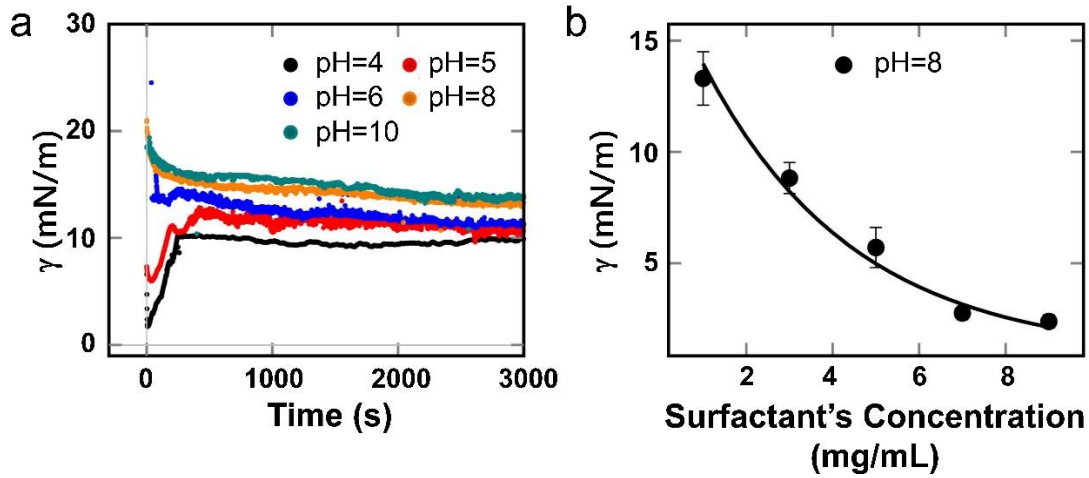

Supplementary Fig. 2. The measurement of the interfacial tension.

a, The time evolution of interfacial tension (γ) between the aqueous and toluene phase as a function of pH. **b,** The equilibrium interfacial tension between the aqueous and toluene phase as a function of surfactant's concentration. The concentrations of Fe_3O_4 nanoparticles and PS-triNH_2 both are 1 mg/mL.

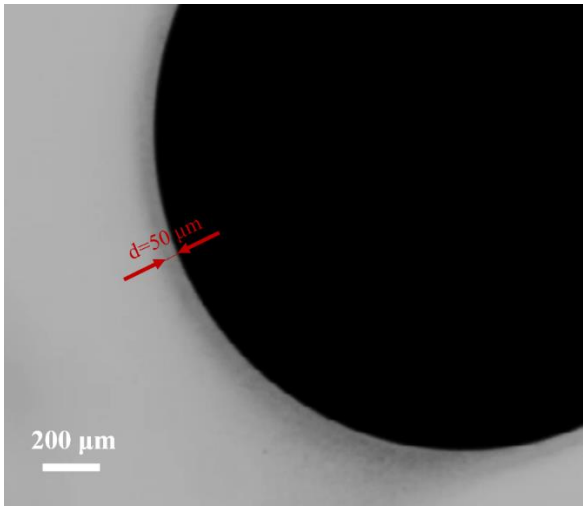

Supplementary Fig. 3. The optical microscopy image of the aqueous droplet/oil interface.

The concentrations of Fe_3O_4 nanoparticles and PS-triNH_2 both are 1 mg/mL. The pH of aqueous phase is 5.

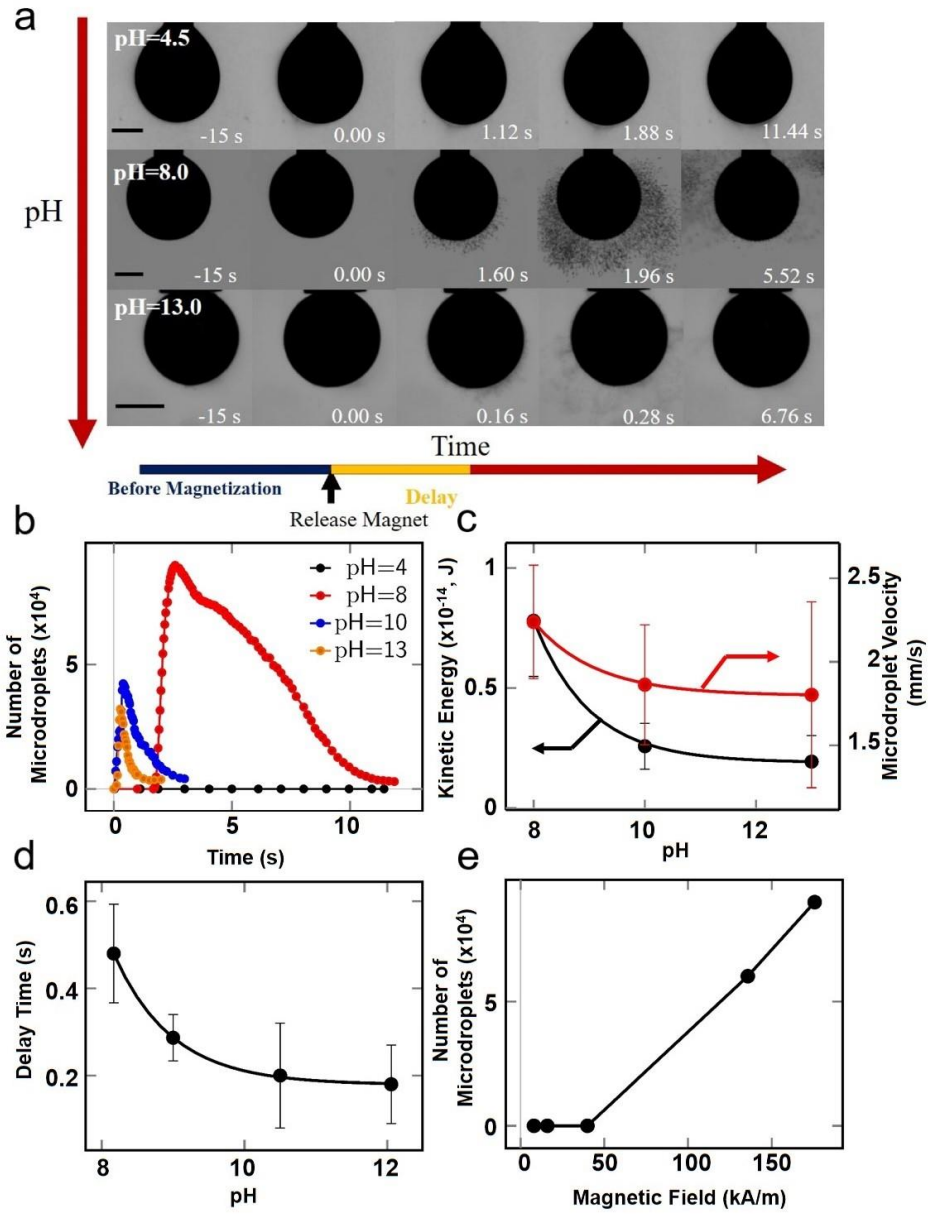

Supplementary Fig. 4. Explosive spontaneous emulsification as a function of pH.

a, The optical images of the aqueous droplets during and after magnetization at different pH. **b,** The temporal changes of the ejected microdroplets' number at different pH. **c,** Ejection velocity and total kinetic energy of the ejected microdroplets as a function of pH. **d,** Effect of pH on the length of delay. **e,** The ejected microdroplets' number triggered at different magnetic field intensity and the pH of aqueous droplet is 8. The concentrations of Fe_3O_4 nanoparticles and PS-triNH_2 both are 1 mg/mL. Scale bar is 500 μm.

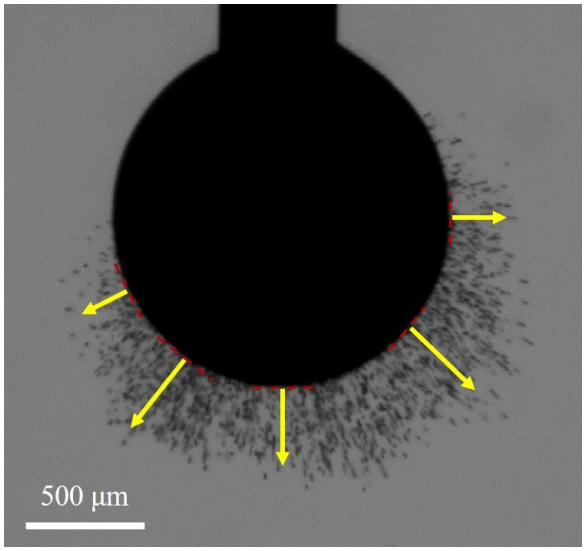

Supplementary Fig. 5. The optical graph of an aqueous droplet occurring explosive spontaneous emulsification.

The red dash lines represent the tangent lines at the surface, and the yellow arrows represent the ejection direction of the emulsions.

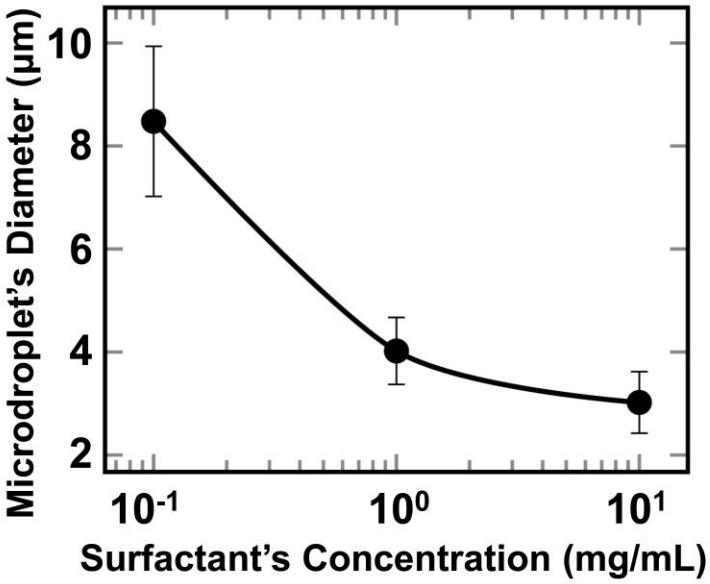

Supplementary Fig. 6. The size of the microdroplet varying with the concentration of the surfactant in oil phase.

The concentrations of Fe_3O_4 nanoparticles are 1 mg/mL, and the pH of the aqueous phase is 5.

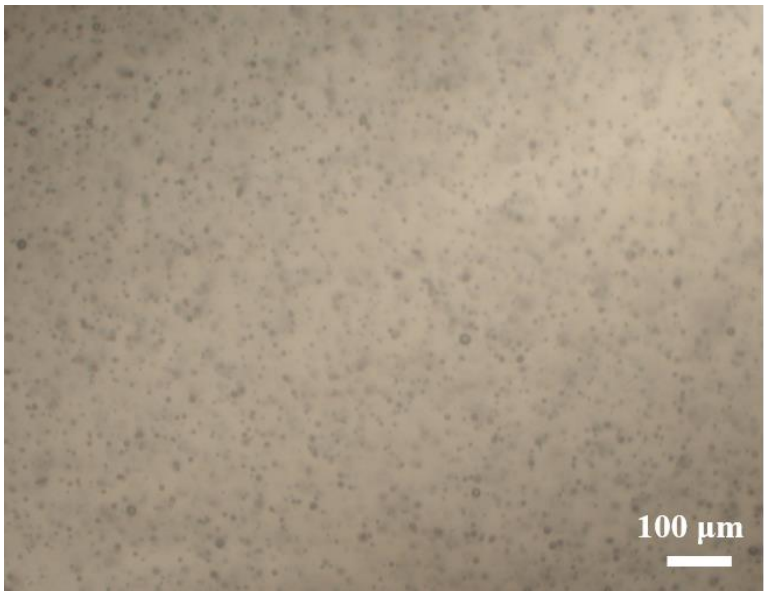

Supplementary Fig. 7. Micrograph of the emulsions stably dispersed in the toluene.
The concentrations of Fe_3O_4 nanoparticles and PS-triNH_2 both are 1 mg/mL.

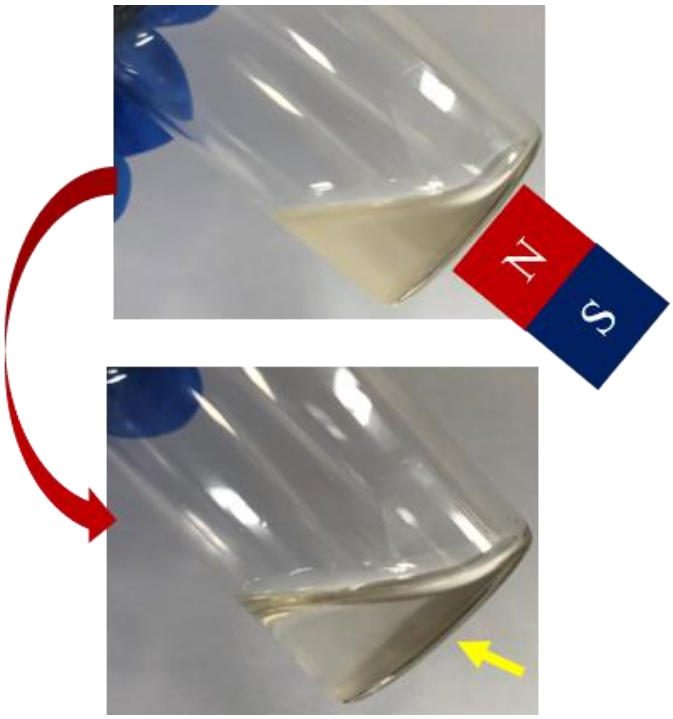

Supplementary Fig. 8. The photographs of the microdroplet dispersions before and after magnetization by the magnet below the vial.
The yellow arrow indicates the microdroplet are attracted by the magnet to the bottom.

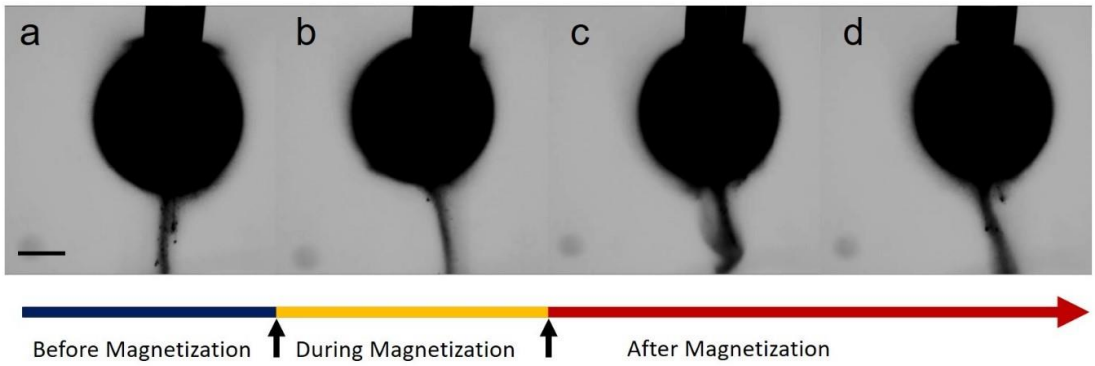

Supplementary Fig. 9. The time serials optical images of the pendant aqueous droplet before, during and after magnetization.

The concentrations of Fe_3O_4 nanoparticles and PS-triNH_2 are 1 mg/mL and 9 mg/mL, respectively. The pH of aqueous phase is 7.

Supplementary Video 1.

Spontaneous emulsification. The concentrations of Fe_3O_4 nanoparticles and PS-triNH_2 are 1 mg/mL and 7 mg/mL, respectively. The pH of aqueous phase is 7.

Supplementary Video 2.

Explosive spontaneous emulsification trigged by the external magnetic field. The concentrations of Fe_3O_4 nanoparticles and PS-triNH_2 are 1 mg/mL and 1 mg/mL, respectively. The pH of aqueous phase is 8.

Supplementary Video 3.

The movement of microdroplets on a magnet stirrer. The concentrations of Fe_3O_4 nanoparticles and PS-triNH_2 are 1 mg/mL and 5 mg/mL, respectively. The pH of aqueous phase is 7. Rotating microdroplets indicated by arrows.

Reference

[1] J. D. Jackson, *Classical electrodynamics; 2nd ed.* (Wiley, New York, NY, 1975).
[2] X. Song, D. Chandler, and R. A. Marcus, J. Phys. Chem. **100**, 11954 (1996).
[3] X. Song and D. Chandler, J. Chem. Phys. **108**, 2594 (1998).
[4] Onsager, L. J. Am. Chem. Soc. **58**, 1486 (1936).
[5] J. D. Weeks, D. Chandler, and H. C. Andersen, J. Chem. Phys. **54**, 5237 (1971).
[6] Q. Li, C. W. Kartikowati, S. Horie, T. Ogi, T. Iwaki, and K. Okuyama, Sci. Rep. **7**, 1 (2017).
[7] A. P. Hynninen and M. Dijkstra, Phys. Rev. Lett. **94**, 138303 (2005).

[8] A. P. Thompson, H. M. Aktulga, R. Berger, D. S. Bolintineanu, W. M. Brown, P. S. Crozier, P. J. in ’t Veld, A. Kohlmeyer, S. G. Moore, T. D. Nguyen, R. Shan, M. J. Stevens, J. Tranchida, C. Trott, and S. J. Plimpton, Comp. Phys. Comm. **271**, 108171 (2022).